# Desensitized Trajectory Optimization for Hypersonic Vehicles

Venkata Ramana Makkapati, Jack Ridderhof, Panagiotis Tsiotras School of Aerospace Engineering Georgia Institute of Technology Atlanta, GA 30332 {mvramana, jridderhof3, tsiotras}@gatech.edu

> Joseph Hart and Bart van Bloemen Waanders Optimization and Uncertainty Quantification Sandia National Laboratories Albuquerque, NM 87123 {joshart, barty}@sandia.gov

#### Abstract

This paper addresses trajectory optimization for hypersonic vehicles under atmospheric and aerodynamic uncertainties using techniques from desensitized optimal control (DOC), wherein open-loop optimal controls are obtained by minimizing the sum of the standard objective function and a first-order penalty on trajectory variations due to parametric uncertainty. The proposed approach is demonstrated via numerical simulations of a minimum-final-time Earth reentry trajectory for an X-33 vehicle with an uncertain atmospheric scale height and drag coefficient. Monte Carlo simulations indicate that dispersions in the final position footprint and the final energy can be significantly reduced without closed-loop control and with little tradeoff in the performance metric set for the trajectory.

## TABLE OF CONTENTS

1 Introduction	. 1
2 HYPERSONIC FLIGHT OVER A SPHERICAL	
PLANET	. 2
3 DESENSITIZED TRAJECTORY OPTIMIZATION	
4 Numerical Results	, ,
5 CONCLUSION	, (
ACKNOWLEDGMENTS	
REFERENCES	
BIOGRAPHY	

#### 1 Introduction

Optimal trajectory planning and feedback control are two critical and interrelated components required to achieve autonomous flight. Traditionally, a nominal trajectory is computed preflight by solving an optimization problem constrained by the vehicle's dynamical model, containing estimated atmospheric and aerodynamic parameters. The guidance law is then given as the sum of this nominal input with a feedback term, which is added so that the trajectory is robust to parametric uncertainties and random disturbances. It follows that, in a clear division of labor, the open-loop nominal control defines the nominal trajectory and the feedback control reduces sensitivity to uncertainty. Take for example the Apollo direct entry guidance, which was designed as part of the Apollo program and later adapted for the Mars Science Laboratory (MSL) and Mars 2020 entry guidance [1–3]. A nominal profile of bank angle commands are first set to determine the nominal entry path, and then feedback gains

are computed as a function of the adjoint system integrated backwards along the nominal trajectory.

In this paper, we propose, instead, to reduce dispersions of hypersonic trajectories due to parametric uncertainties by selection of the *nominal* trajectory. The nominal control then serves a dual role of optimizing the given performance metric *and* reducing dispersions. In particular, the desensitized optimal control (DOC) framework [4,5] is used to construct cost regularizers to generate trajectories which are less sensitive to parametric variations, while trading off nominal performance for robustness to parametric uncertainties.

Early work on *trajectory sensitivity design* include those of Winsor and Roy [6], who developed a technique to design controllers that provide assurance for system performance under mathematical modeling inaccuracy. The feasibility of the technique was established with appropriate simulation results. Following that work, several approaches including sensitivity-reduction for linear regulators, using increased-order augmented system [7], modification of weighting matrix [8], feedback [9, 10], and an augmented cost function [11,12], were all thoroughly analyzed. The approach of using an augmented cost function was further tested on the linear quadratic regulator (LQR) problem, which was later applied for active suspension control in passenger cars [12].

With the work on trajectory sensitivity design mostly restricted to analyzing linear systems, more recent approaches under the title DOC considered sensitivities to address dispersions under modeling uncertainties in general nonlinear optimal control problems. The work by Seywald et al. makes use of sensitivity analysis to obtain an optimal openloop trajectory that is insensitive to first-order parametric variations for general optimal control problems [13, 14]. The proposed approach elevates the parameters of interest to system states, and defines a binary sensitivity function that provides the first-order variation in the states at time t, given the variation in the states at some time t' ( $t' \leq t$ ). An appropriate sensitivity cost is added to the existing cost function, and the dynamics of the binary sensitivity function is augmented in the system dynamics to solve the resulting optimal control problem. The approach was later extended to optimal control problems with control constraints [15], and it was used to solve the Mars pinpoint landing problem [16]. Some extensions to the landing problem include considering uncertainties in atmospheric density and aerodynamic characteristics [17], and the use of direct collocation and nonlinear programming [18].

An alternative approach was presented by Makkapati et al. [4] wherein the dimensionality of the state-space for the augmented problem is reduced using traditional sensitivity functions. A sensitivity function provides information about the first order variation of the state under parameter variations at a given time instant along the trajectory. The sensitivity function follows linear dynamics, expressed using the partial derivatives of the state dynamics with respect to the state and the parameter, along a given trajectory. The components of the sensitivity function are first augmented to the original state vector. By appropriately regularizing the entries of the sensitivity function, it is demonstrated that the dispersion in the optimal trajectory or the state at a particular time instant (for example, the final state) can be significantly reduced.

On another research direction, recent works have considered hypersonic guidance as a stochastic control problem with the atmospheric density considered to be a random process [19, 20]. In this framework, the vehicle trajectory is a random process with statistics determined by the guidance law, and both the nominal control and the feedback gains may then be jointly optimized subject to probabilistic constraints [21, 22]. Aerocapture guidance has similarly been considered as a stochastic problem with a finite set of uncertain parameters [23].

The main contribution of this work is to tailor the DOC techniques [4] for hypersonic vehicle trajectory optimization with a principled approach to appropriately penalize sensitivity functions, and to this end, we derive inspiration from the stochastic approaches. We will show that penalizing the sensitivity matrix is equivalent to minimizing an expected quadratic error, provided that the uncertain parameters are given as a Gaussian distributed random vector. The penalty on the sensitivity matrices may then be derived as a function of the assumed parameter covariance and the user-defined weight on expected output variations.

## 2 HYPERSONIC FLIGHT OVER A SPHERICAL PLANET

The motion of a vehicle in unpowered, atmospheric flight around a spherical, non-rotating planet is described by the system of ordinary differential equations

$$\dot{r} = v \sin \gamma, \tag{1a}$$

$$\dot{\theta} = \frac{v \cos \gamma \sin \psi}{r \cos \phi},\tag{1b}$$

$$\dot{\phi} = \frac{v\cos\gamma\cos\psi}{r},\tag{1c}$$

$$\dot{v} = -\frac{D}{m} - \frac{\mu \sin \gamma}{r^2},\tag{1d}$$

$$\dot{\gamma} = \frac{L\cos\sigma}{mv} - \frac{\mu\cos\gamma}{r^2v} + \frac{v}{r}\cos\gamma,\tag{1e}$$

$$\dot{\psi} = \frac{L\sin\sigma}{mv\cos\gamma} + \frac{v}{r}\cos\gamma\sin\psi\tan\phi,\tag{1f}$$

where r is the radial distance from the center of the planet to the vehicle,  $\theta$  and  $\phi$  are the longitude and latitude, respectively, v is the planet-relative velocity,  $\gamma$  is the planet-relative flight path angle, and  $\psi$  is the planet-relative heading azimuth. The bank angle  $\sigma$  is the angle between the lift vector and the local vertical measured about the velocity vector, measured positive to the right;  $\mu$  is the planet's gravitational parameter;

m is the vehicle mass, which is assumed to be constant; and the lift force L and drag force D are given as

$$L = \rho v^2 C_L(\alpha) S/2, \quad D = \rho v^2 C_D(\alpha) S/2, \quad (2)$$

in terms of the atmospheric density  $\rho$ , the reference area S, and the lift and drag coefficients  $C_L$  and  $C_D$ , which are functions of the angle of attack  $\alpha$ . The density is assumed to be an exponential function of the altitude as

$$\rho(r) = \rho_0 \exp\left(-\frac{r - r_p}{H_s}\right),\tag{3}$$

where  $r_p$  is the radius at the surface of the planet,  $\rho_0$  is the density at the surface, and  $H_s$  is the scale height. We remark that the planet rotation may be taken into account by allowing for time-dependent targeting constraints.

The vehicle's trajectory is constrained by the heating rate  $\dot{Q}$ , dynamic pressure q, and normal load n as follows: [24]

$$\dot{Q} = k_O \sqrt{\rho} v^3 \le \dot{Q}_{\text{max}},\tag{4a}$$

$$q = \frac{1}{2}\rho v^2 \le q_{\text{max}},\tag{4b}$$

$$n = \sqrt{L^2 + D^2}/m \le n_{\text{max}},\tag{4c}$$

where  $k_Q$  is a constant, and where the maximum values  $\dot{Q}_{\rm max}$ ,  $q_{\rm max}$ , and  $n_{\rm max}$  are determined by the vehicle characteristics.

Let the bank angle and the angle of attack be the control inputs for the purposes of trajectory control; accordingly, we set

$$u = (\sigma, \alpha). \tag{5}$$

Similarly, we let x be the state vector given as

$$x = (r, \theta, \phi, v, \gamma, \psi). \tag{6}$$

# 3 DESENSITIZED TRAJECTORY OPTIMIZATION

Consider the following trajectory optimization problem: Find the control u(t) and the final time  $t_f$  that minimize the cost

$$\mathcal{J}(u,t_f) = \Gamma(x(t_f),t_f) + \int_{t_0}^{t_f} \mathcal{L}(x(t),u(t),t) \,\mathrm{d}t, \quad (7)$$

subject to the dynamics (1), along with the constraints in (4) and

$$\Psi(x(t_f), t_f) = 0. \tag{8}$$

Here,  $\Gamma$  is the terminal cost,  $\mathcal{L}$  is the running cost, and the vector-valued function  $\Psi$  defines the terminal condition at the final time.

Suppose that the control which minimizes the objective (7), subject to the dynamics and the path constraints, is identified. Then the resulting optimal trajectory depends on both this control input and on select, uncertain parameters of interest in the system, such as the aerodynamic model or the atmospheric model; these parameters will be represented by the  $\ell$ -dimensional vector p. We denote this dependence by writing

the state, whose dependence on the control u is suppressed for notational convenience, as

$$x(p,t), (9)$$

which is the solution to the dynamical equations in (1) along with appropriate initial conditions, which we rewrite as

$$\dot{x} = f(x, p, u, t), \quad x(t_0) = x_0.$$
 (10)

The assumed (nominal) values of the parameters will be denoted  $\hat{p}$ , and the corresponding nominal trajectory is  $x(\hat{p},t)$ .

Since the parameters are assumed to be equal to their nominal values for the purposes of solving for the optimal control input, it will be useful to quantify how perturbations in the parameters from the nominal values affects the resulting vehicle trajectory. We will make use of the well-known first-order approximation of the deviation of the trajectory x(p,t) from its nominal value  $x(\hat{p},t)$  [25]

$$x(p,t) - x(\hat{p},t) \approx S(t)(p - \hat{p}), \tag{11}$$

where S(t) is the so called sensitivity function, which is obtained as the solution to the ordinary differential equation [4]

$$\dot{S}(t) = A(t)S(t) + B(t), \quad S(t_0) = 0, \tag{12}$$

where the matrices A(t) and B(t) are the derivatives of the dynamics with respect to the state and the parameters, respectively, evaluated along the nominal trajectory  $x(\hat{p}, t)$ :

$$A(t) = \frac{\partial f}{\partial x} (x(\hat{p}, t), \hat{p}, u(t), t), \tag{13}$$

$$B(t) = \frac{\partial f}{\partial n} (x(\hat{p}, t), \hat{p}, u(t), t). \tag{14}$$

Since A(t) and B(t) are evaluated along the nominal trajectory  $x(\hat{p},t)$ , which is a function of the control inputs, the sensitivity function may be affected by the selection of the control inputs, and we may therefore seek controls which result in trajectories which are less sensitive to parametric variations. The study of finding such controls is known as desensitized optimal control [5,26].

To this end, let y be an output vector, whose variations are of concern, given as a function of the state by

$$y = g(x). (15)$$

Suppose that the uncertain parameters are Gaussian distributed as

$$p \sim N(\hat{p}, P),\tag{16}$$

where P is a fixed and known positive semi-definite matrix. We then modify the nominal objective function (7) to include a sensitivity penalty in the form of the expected quadratic error of the output:

$$\mathcal{J}_{D}(u, t_{f}) = \mathcal{J}(u, t_{f}) + \mathbb{E}\left(\|\delta y(t_{f})\|_{Q_{f}}^{2} + \int_{t_{0}}^{t_{f}} \|\delta y(t)\|_{Q(t)}^{2} dt\right), \quad (17)$$

where Q(t) and  $Q_f$  are both user-defined, positive semi-definite weight matrices penalizing output dispersions along the trajectory and at the final time, respectively.

Next, we approximate the stochastic error term in (17) using a first-order approximation in terms of the sensitivity function. The variation of the output parameter from its nominal value is approximated by

$$\delta y = g(x) - g(\hat{x}) \approx G\delta x \approx GS\delta p,$$
 (18)

where G is the Jacobian of g evaluated at the nominal state value  $\hat{x}(t) = x(\hat{p},t)$ ,  $\delta x(t) = x(p,t) - x(\hat{p},t)$  and  $\delta p = p - \hat{p}$ , and we drop explicit dependence on time for notational convenience. The stochastic error terms in (17) may therefore be given as a function of the sensitivity matrix by

$$\mathbb{E}(\|\delta y\|_{Q}^{2}) = \operatorname{tr} Q \mathbb{E}(\delta y \delta y^{\mathsf{T}}) \approx \operatorname{tr} Q G S P S^{\mathsf{T}} G^{\mathsf{T}}, \tag{19}$$

where, with a slight abuse of notation, Q can refer to either the running weight matrix Q(t) or the final weight matrix  $Q_f$ . The cost (17) is now approximated in terms of the sensitivity function in such a way that the output-error weight Q and parameter covariance P determine the relative weight placed on the stochastic error term as compared to the nominal cost. If the output-error weight Q is held constant, for example, then an increase in the parameter uncertainty, by means of the parameter covariance matrix P increasing, will result in a larger weight placed on the sensitivity matrix compared to the nominal cost. Conversely, in an extreme case, when the parameter uncertainty decreases to zero, the optimization will approach a standard trajectory optimization problem.

Desensitization for Hypersonic Trajectory Optimization

Consider now the problem of solving for desensitized hypersonic vehicle trajectories. Since the vehicle aerodynamics and the atmospheric density are both uncertain and they greatly impact vehicle trajectories [27, 28], we will consider desensitization with respect to the aerodynamic and atmospheric density models. In particular, we model the vehicle aerodynamics by the relationship

$$C_D = C_{D_0} + KC_L^N, (20)$$

where the values  $C_{D_0}$ , K, and N depend on the vehicle model, and where  $C_{D_0}$  is referred to as the parasitic drag coefficient. The lift coefficient is assumed to be a continuous and monotonic function of the angle of attack, and hence  $C_L(\alpha)$  is bijective. We may therefore optimize over  $C_L$  in place of  $\alpha$ .

Henceforth, the parasitic drag coefficient  $C_{D_0}$  from (20) and the scale height  $H_s$  from (3) will be considered as uncertain parameters:

$$p = (C_{D_0}, H_s).$$
 (21)

The trajectory deviation approximation (11) for the hypersonic problem is thus given as

$$\begin{bmatrix}
\delta r(t) \\
\delta \theta(t) \\
\delta \phi(t) \\
\delta \phi(t) \\
\delta v(t) \\
\delta \gamma(t) \\
\delta \psi(t)
\end{bmatrix} \approx
\begin{bmatrix}
S_{r,C_{D_0}}(t) & S_{r,H_s}(t) \\
S_{\theta,C_{D_0}}(t) & S_{\theta,H_s}(t) \\
S_{\phi,C_{D_0}}(t) & S_{\phi,H_s}(t) \\
S_{v,C_{D_0}}(t) & S_{v,H_s}(t) \\
S_{\gamma,C_{D_0}}(t) & S_{\gamma,H_s}(t) \\
S_{\psi,C_{D_0}}(t) & S_{\psi,H_s}(t)
\end{bmatrix} \begin{bmatrix}
\delta C_{D_0} \\
\delta H_s
\end{bmatrix}.$$
(22)

For this study, the perturbations in the final longitude, final latitude, and final final mass-specific energy

$$e = \frac{v^2}{2} - \frac{\mu}{r},\tag{23}$$

were penalized. The output vector y is accordingly set to be

$$y = (\theta, \ \phi, \ e). \tag{24}$$

The first-order approximation of the energy error is given as

$$\delta e \approx \frac{\mu}{r^2} \delta r + v \delta v,$$
 (25)

which is obtained by differentiating (23), and therefore the Jacobian G of the mapping y=g(x) is

$$G = \begin{bmatrix} 0 & 1 & 0 & 0 & 0 & 0 \\ 0 & 0 & 1 & 0 & 0 & 0 \\ \mu/r^2 & 0 & 0 & v & 0 & 0 \end{bmatrix}.$$
 (26)

#### 4 NUMERICAL RESULTS

In this section, we apply the DOC methodology to an example Earth reentry scenario using the X-33 vehicle model [29,30]. The initial and target states are listed in Table 1, and the vehicle specification is given in Table 2. The lift coefficient and the bank angle are constrained by  $-0.15 \leq C_L \leq 0.8$  and  $-90^{\circ} \leq \sigma \leq 90^{\circ}$ , and their rates are bounded by  $\pm 0.05$  s $^{-1}$  and  $\pm 5$  deg/s, respectively. Note that  $h=r-r_p$  denotes the altitude of the vehicle. The radius of Earth is  $r_p=6,371$  km, the surface density is  $\rho_0=1.225$  kg/m³, the gravitational parameter is  $\mu=3.986\times 10^{14}$  m³/s², the nominal scale height is  $H_s=7,254.24$  m, and the constant that is used to obtain heating rate in (4a) is  $k_Q=9.4369\times 10^{-5}$  kg $^{0.5}/\text{m}^{1.5}$ .

The angle of attack (equivalently, the lift coefficient) and the bank angle profiles were set to minimize the final time, subject to the boundary conditions and the path constraints. The parasitic drag coefficient and the scale height are assumed to be Gaussian distributed with the mean value  $\hat{C}_{D_0}$  listed in Table 2 and the mean value  $\hat{H}_s$  as above, and with variances set so that their  $3\sigma$  variations are equal to 2% of their nominal values:

$$\begin{bmatrix} C_{D_0} \\ H_s \end{bmatrix} \sim N \left( \begin{bmatrix} \hat{C}_{D_0} \\ \hat{H}_s \end{bmatrix}, \frac{0.02^2}{3^2} \begin{bmatrix} \hat{C}_{D_0}^2 & 0 \\ 0 & \hat{H}_s^2 \end{bmatrix} \right). \tag{27}$$

The output-error weight matrix at the final time  $Q_f$  equally weights the longitude error, latitude error, and non-dimensionalized energy, which, when given dimensionalized units is equal to

$$Q_f = \beta \begin{bmatrix} 1 & 0 & 0 \\ 0 & 1 & 0 \\ 0 & 0 & 1/r_p g_0 \end{bmatrix}, \tag{28}$$

where  $\beta$  is a user-defined, desensitization-weight parameter, and where  $g_0=9.81~\mathrm{m/s^2}$  is the gravitational acceleration at the Earth's surface.

The desensitized trajectory is obtained by minimizing the cost (17) with Q(t)=0 and  $Q_f$  as in (28) with  $\beta=3$ ; a baseline trajectory was similarly solved except with  $\beta=0$  (i.e., no desensitization). To improve numerical performance, the problem is first non-dimensionalized with lengths and time being scaled by  $r_p$  (radius of the Earth) and  $\sqrt{r_p/g_0}$  ( $g_0$  is the Earth gravitational acceleration at  $r_p$ ), respectively. The optimal control problem is then solved using GPOPS-II [31]. The baseline and the desensitized state trajectories

Table 1. Initial and final vehicle state

State	Initial Value	Final Value	Units
h	121.9	30.48	km
$\theta$	-123	-81	$\deg$
$\phi$	-25	28.61	deg
v	7626	908.15	m/s
$\gamma$	-1.25	[-6, 0]	deg
$\psi$	45	90	deg

Table 2. X-33 vehicle parameters

Parameter	Value	Units
S	149.3881	$m^2$
m	38000	kg
$\dot{Q}_{max}$	$4 \times 10^{5}$	$W/m^2$
$q_{max}$	14500	kg/ms <sup>2</sup>
$n_{\mathrm{max}}$	$5g_0$	m/s <sup>2</sup>
$C_{D_0}$	0.12	-
K	1.125	-
N	1.9	-

are shown in Figure 1 and the groundtracks are shown in Figure 2; the control histories are given Figure 3; and the dynamic pressure, load factor, and heating rate histories are shown in Figure 4.

Both the baseline and the desensitized trajectories exhibit phugoid oscillations, as expected for a high-L/D vehicle; however, the baseline and the desensitized trajectories noticeably diverge following the first peak in dynamic pressure around 300 s. The baseline bank angle slowly decreases from being mostly lift up to having zero lift up after 1,000 s, and then a single bank reversal is performed while holding zero vertical lift. Shortly following the time that the baseline bank angle is at  $-90^{\circ}$  — that is, when the vehicle removes any component vertical lift to aggravate its descent — the baseline trajectory reaches maximum load factor and dynamic pressure. Interestingly, in contrast, the desensitized bank angle reaches  $-90^{\circ}$  (zero vertical lift) after only  $\sim\!400\,\mathrm{s}$ , and then the desensitized trajectory follows an irregular path of oscillating velocity and altitude.

The sensitivity functions, as defined in (22), are plotted in Figures 6 and 7, wherein the effect of the desensitization is shown; the sensitivity of the final longitude and latitude to both the parasitic drag coefficient and the scale height are clearly decreased when compared to the baseline trajectory. When plotting the altitude against the velocity, as shown in Figure 4, we see that the desensitized trajectory slows down to  $4 \, \mathrm{km/s}$  at a higher altitude before rapidly descending. The trajectory sensitivity at around this time (~950 s), when the desensitized trajectory passes through  $4 \, \mathrm{km/s}$ , the absolute value of the sensitivity of the longitude and latitude to both  $C_{D_0}$  and  $H_s$  along the desensitized trajectory begins to rapidly decrease, as can be seen in Figures 6 and 7.

Next, we ran a 1,000 trial Monte Carlo simulation with the parameters sampled from the Gaussian distribution as in (27). In the following, all of the Monte Carlo samples are used to calculate a sample mean and covariance, but only 100

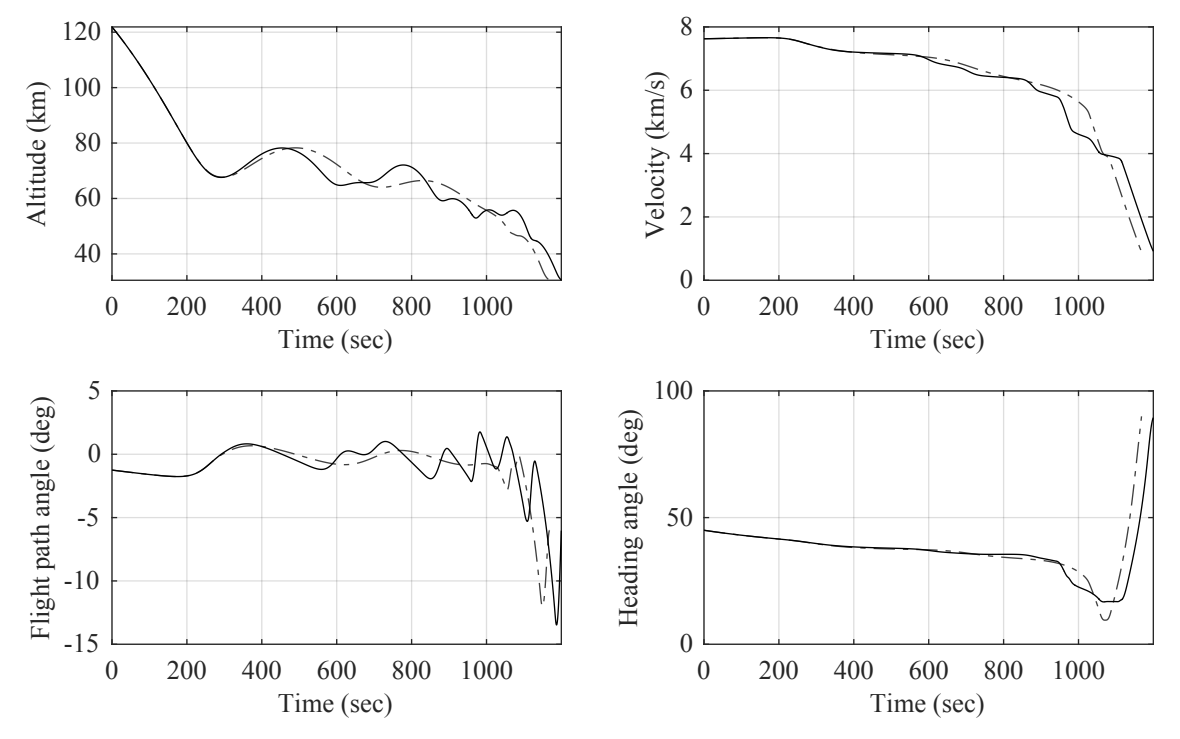


Figure 1. Baseline (gray, dashed) and desensitized (black) trajectories.

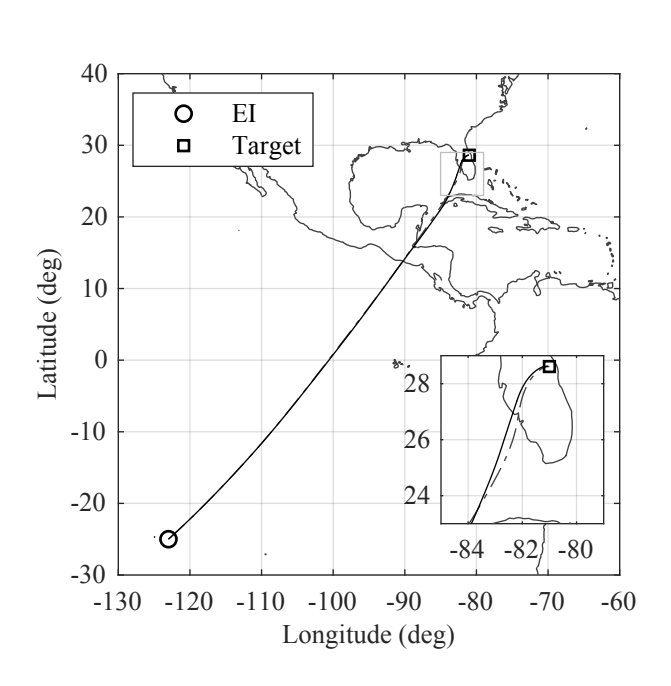


Figure 2. Baseline (gray, dashed) and desensitized (black) trajectory groundtracks.

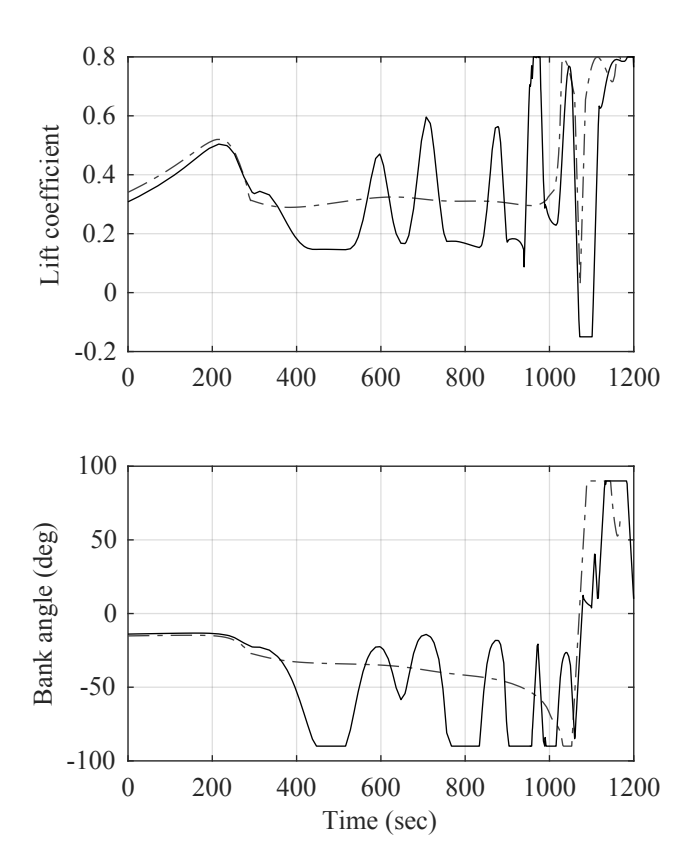


Figure 3. Baseline (gray, dashed) and desensitized (black) control histories.

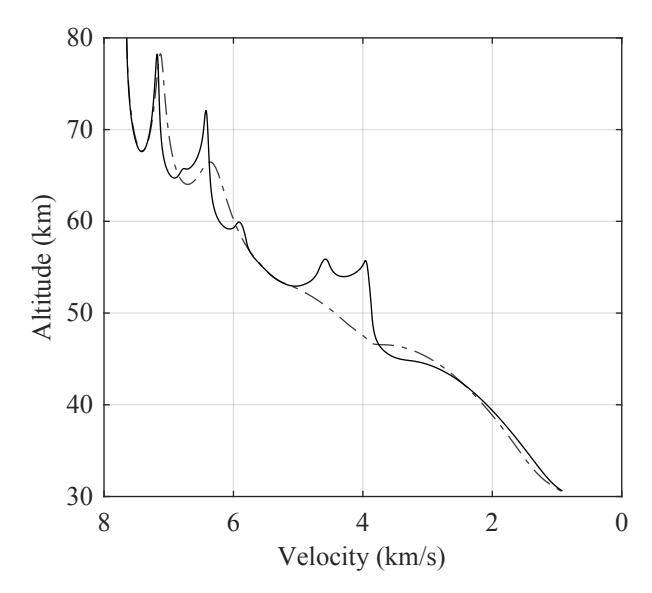


Figure 4. Baseline (gray, dashed) and desensitized (black) trajectories.

samples are shown in scatter plots for visual clarity. Sample values of the parameters are shown in Figure 8, samples of the final longitude and latitude error are shown in Figure 9, and samples of the final altitude and velocity error are shown in Figure 10. The  $3\sigma$  confidence ellipses in Figures 9 and 10 are computed from the sample mean and sample covariance of the 1,000 Monte Carlo trials; that is, the probability a sample lies in the ellipse, provided that the sample were Gaussian with the mean and covariance equal to the sample mean and covariance, is 99.97%. In Figure 9, we see that the dispersed footprint of the desensitized trajectory is significantly less than the baseline trajectory: The semi-major axis of the  $3\sigma$  confidence ellipse of the desensitized trajectory footprint is  $3.34~{\rm km}$  compared to  $26.37~{\rm km}$  for the baseline trajectory.

The final altitude and velocity errors shown in Figure 10 similarly show the desensitized trajectory clearly results in lower dispersions. In this case, and in contrast to the longitude and latitude dispersions in Figure 9, the desensitized trajectory results in a different correlation between final velocity and final altitude error when compared to the baseline trajectory. This follows from our penalty on the final energy, which imposed a relative weighting on the altitude and the velocity penalty via the G matrix in (19). Finally, histograms of the final energy error for both the baseline and the desensitized trajectory are shown in Figure 11; it can be seen that the desensitized trajectory has significantly decreased the final energy error. This decrease in the final energy error will be useful in practice, since terminal guidance is often responsible for energy management leading to landing [32].

### 5 CONCLUSION

The paper presents a principled method to construct a cost regularizer using sensitivity functions that captures output variations up to first order under parametric uncertainties. The approach is applied on a trajectory optimization problem for hypersonic vehicles under model uncertainties. A time-optimal control formulation is considered for the X-33 model under Earth entry conditions, and the variations in position and energy at the final time are penalized. Numerical

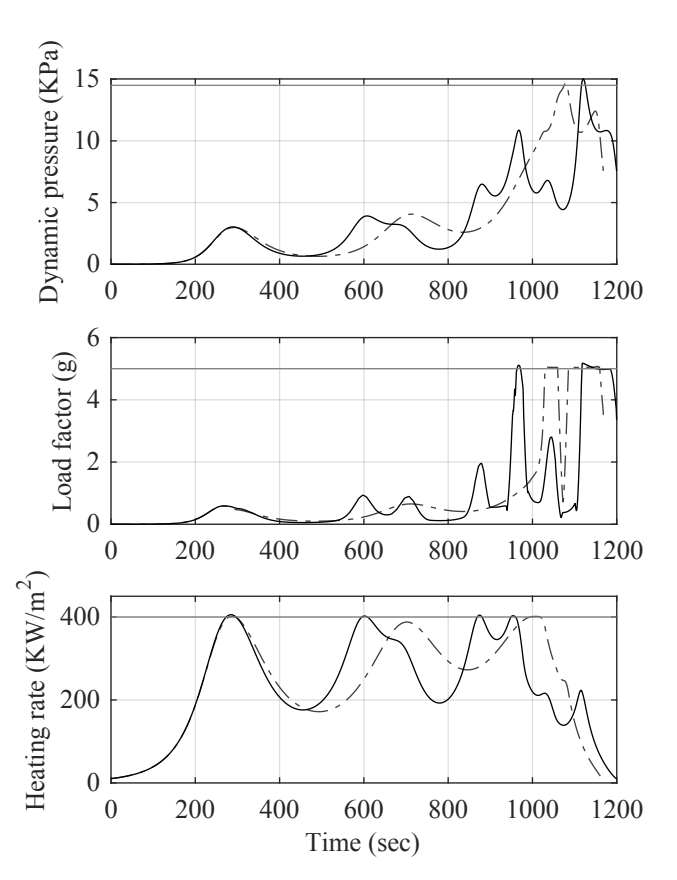


Figure 5. Baseline (gray, dashed) and desensitized (black) dynamic pressure, load factor, and hating rate histories with the maximum allowable values (gray).

experiments suggest that trade-offs between optimality and robustness against parametric variations can be efficiently obtained using the proposed approach.

### **ACKNOWLEDGMENTS**

Any subjective views or opinions that might be expressed in the paper do not necessarily represent the views of the U.S. Department of Energy or the United States Government. The work is funded by Sandia National Laboratories, which is a multimission laboratory managed and operated by National Technology and Engineering Solutions of Sandia LLC, a wholly owned subsidiary of Honeywell International, Inc., for the U.S. Department of Energy's National Nuclear Security Administration under contract DE-NA-0003525. SAND2020-11208 C. The work of the second author is supported by a NASA Space Technology Research Fellowship.

### REFERENCES

- [1] P. E. Moseley, "The Apollo entry guidance: A review of the mathematical development and its operational characteristics," TRW Note No. 69-FMT-791, December 1969.
- [2] G. L. Carman, D. G. Ives, and D. K. Geller, "Apolloderived precision lander guidance," in 23rd Atmospheric Flight Mechanics Conference, no. 98-4570, Boston, MA 1998
- [3] G. F. Mendeck and L. Craig McGrew, "Entry guidance design and postflight performance for 2011 Mars Sci-

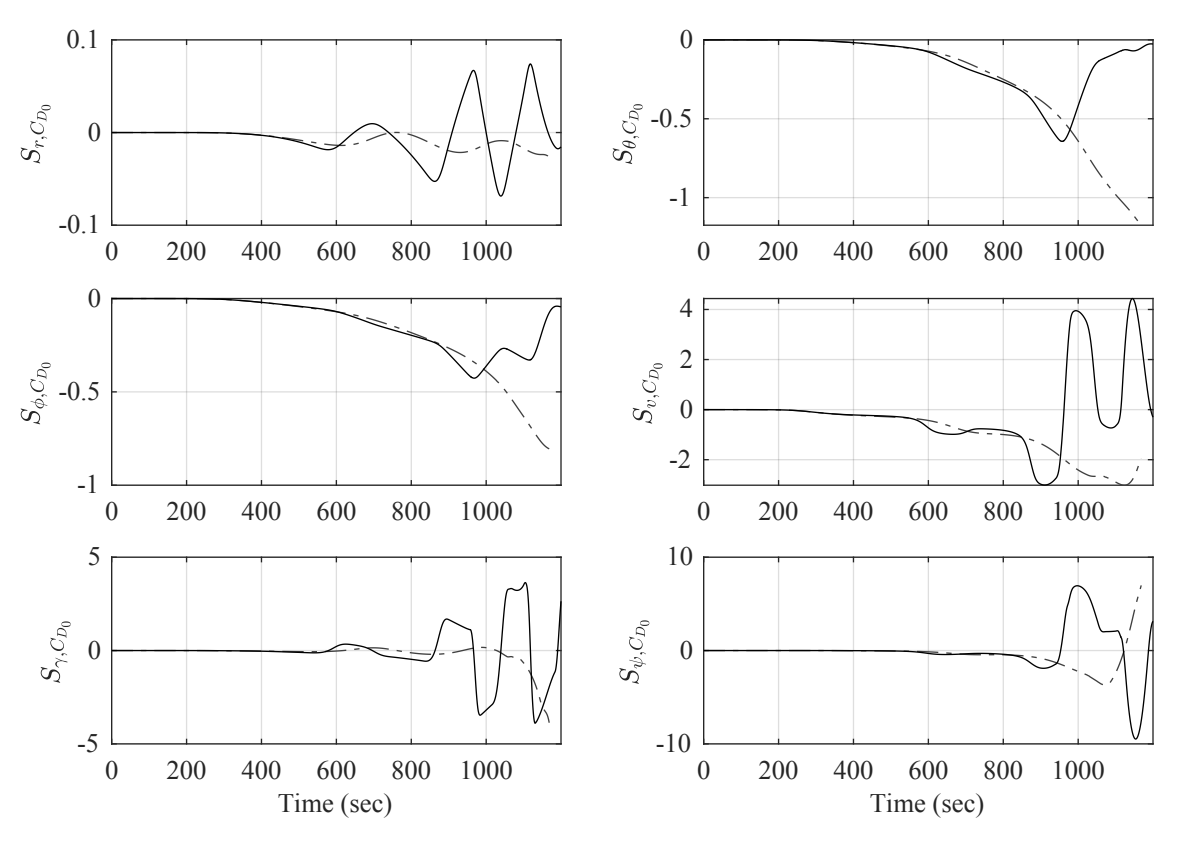


Figure 6. Baseline (gray, dashed) and desensitized (black) sensitivity functions with respect to  $C_{D_0}$ .

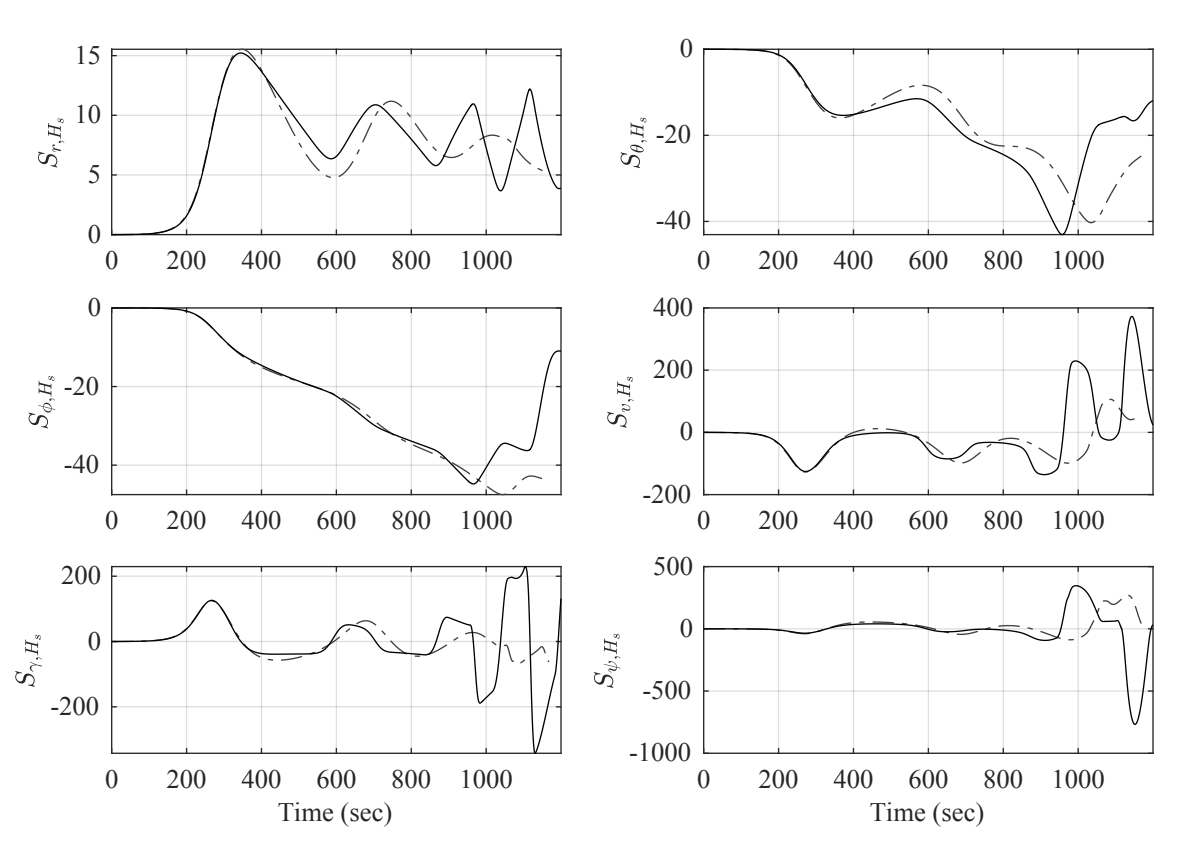


Figure 7. Baseline (gray, dashed) and desensitized (black) sensitivity functions with respect to  $H_s$ .

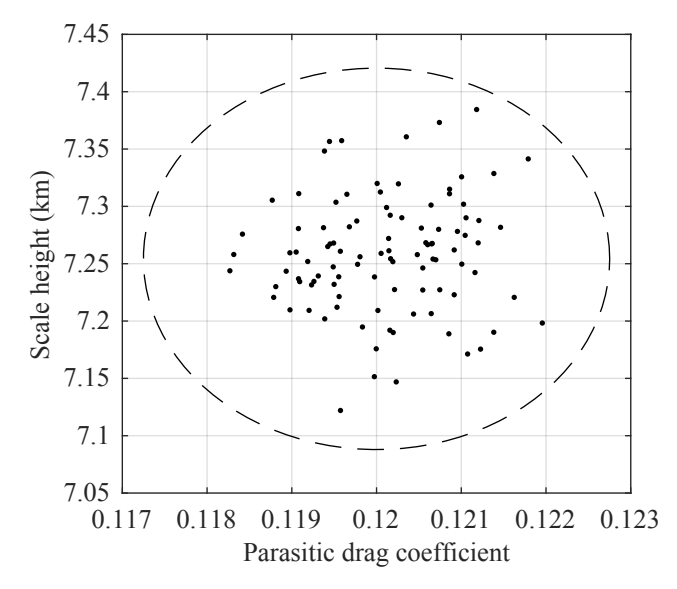


Figure 8. Parameter samples used for Monte Carlo with a  $3\sigma$  confidence bound.

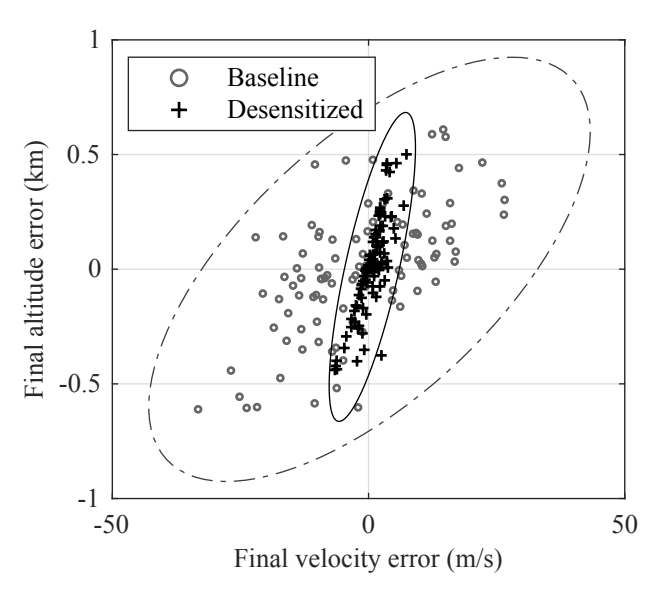


Figure 10. Baseline and desensitized final altitude and velocity errors with  $3\sigma$  confidence bounds.

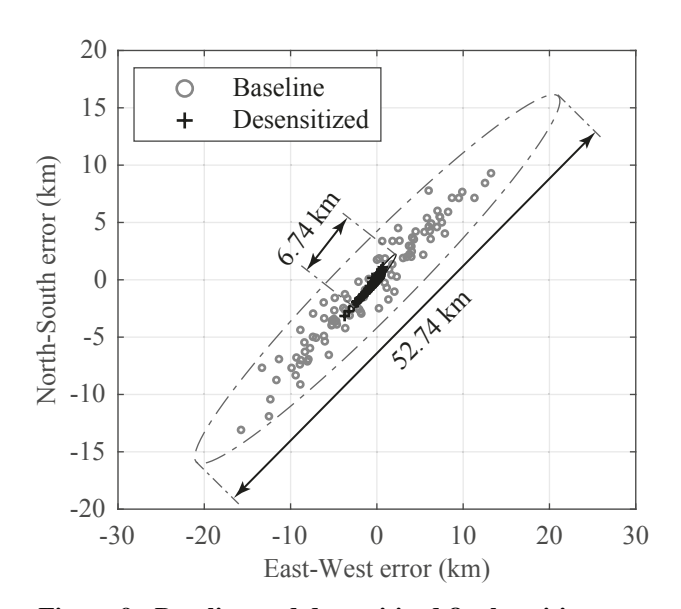


Figure 9. Baseline and desensitized final position errors with  $3\sigma$  confidence bounds.

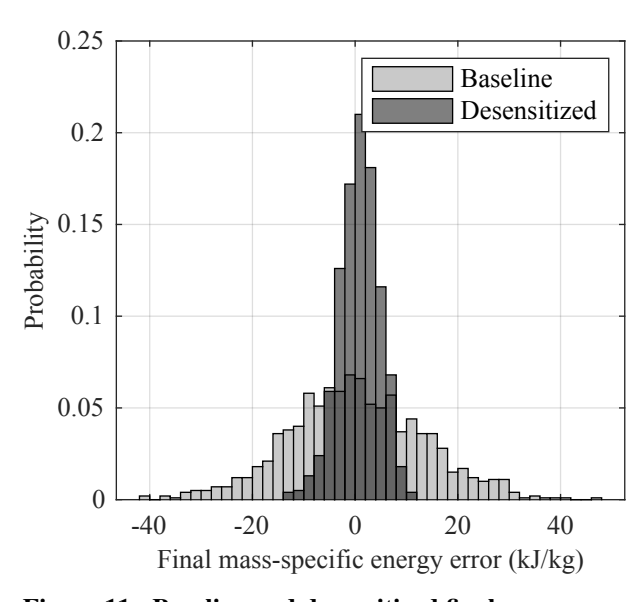


Figure 11. Baseline and desensitized final energy sample distributions.

- ence Laboratory mission," *Journal of Spacecraft and Rockets*, vol. 51, no. 4, pp. 1094–1105, 2014.
- [4] V. R. Makkapati, M. Dor, and P. Tsiotras, "Trajectory desensitization in optimal control problems," in *IEEE Conference on Decision and Control*, Miami, FL, 2018, pp. 2478–2483.
- [5] V. R. Makkapati, H. Sarabu, V. Comandur, P. Tsiotras, and S. Hutchinson, "Safe optimal control under parametric uncertainties," *IEEE Robotics and Automation Letters*, vol. 5, no. 4, pp. 5725–5731, 2020.
- [6] C. Winsor and R. Roy, "The application of specific optimal control to the design of desensitized model following control systems," *IEEE Transactions on Automatic Control*, vol. 15, no. 3, pp. 326–333, 1970.
- [7] R. Subbayyan, V. V. S. Sarma, and M. C. Vaithilingam,

- "An approach for sensitivity-reduced design of linear regulators," *International Journal of Systems Science*, vol. 9, no. 1, pp. 65–74, 1978.
- [8] C. Verde and P. M. Frank, "Sensitivity reduction of the linear quadratic regulator by matrix modification," *International Journal of Control*, vol. 48, no. 1, pp. 211– 223, 1988.
- [9] G. Zames, "Feedback and optimal sensitivity: Model reference transformations, multiplicative seminorms, and approximate inverses," *IEEE Transactions on Automatic Control*, vol. 26, no. 2, pp. 301–320, April 1981.
- [10] B.-C. Chang and J. Pearson, "Optimal disturbance reduction in linear multivariable systems," *IEEE Transactions on Automatic Control*, vol. 29, no. 10, pp. 880–887, Oct 1984.

- [11] D. L. Tang, "The design of a desensitized controller a sensitivity function approach," in *Proceedings of the American Control Conference*, May 1990, pp. 3103–3111.
- [12] F. Cheli, F. Resta, and E. Sabbioni, "Observer design for active suspension control for passenger cars," in Proceedings of the ASME Conference on Engineering System Design and Analysis, Torino, Italy, 2006, pp. 1– 9.
- [13] H. Seywald and R. R. Kumar, "Desensitized optimal trajectories," *Advances in the Astronautical Sciences*, vol. 93, pp. 103–115, 1996.
- [14] K. Seywald and H. Seywald, "Desensitized optimal control," in AIAA SciTech Forum, San Diego, CA, January 2019, aIAA Paper 2019-0651.
- [15] H. Seywald, "Desensitized optimal trajectories with control constraints," *Advances in the Astronautical Sciences*, vol. 114, pp. 737–743, 2003.
- [16] H. Shen, H. Seywald, and R. W. Powell, "Desensitizing the minimum-fuel powered descent for Mars pinpoint landing," *Journal of Guidance, Control, and Dynamics*, vol. 33, no. 1, pp. 108–115, 2010.
- [17] H. Xu and H. Cui, "Robust trajectory design scheme under uncertainties and perturbations for Mars entry vehicle," in *IEEE International Conference on Compu*tational Intelligence Communication Technology, 2015, pp. 762–766.
- [18] S. Li and Y. Peng, "Mars entry trajectory optimization using DOC and DCNLP," *Advances in Space Research*, vol. 47, no. 3, pp. 440–452, 2011.
- [19] J. Ridderhof and P. Tsiotras, "Stochastic atmosphere modeling for risk adverse aerocapture guidance," in 2020 IEEE Aerospace Conference, Big Sky, MT, 2020.
- [20] —, "Planetary entry in a randomly perturbed atmosphere," in AIAA Guidance, Navigation, and Control Conference (Accepted), 2021.
- [21] J. Ridderhof, K. Okamoto, and P. Tsiotras, "Nonlinear uncertainty control with iterative covariance steering," in 2019 IEEE 58th Conference on Decision and Control (CDC), Nice, France, Dec. 2019.
- [22] J. Ridderhof, J. Pilipovsky, and P. Tsiotras, "Chance-constrained covariance control for low-thrust minimum-fuel trajectory optimization," in 2020 AAS/AIAA Astrodynamics Specialist Conference, Aug. 2020.
- [23] C. R. Heidrich and R. D. Braun, "Aerocapture trajectory design in uncertain entry environments," in AIAA Scitech 2020 Forum, Orlando, FL, 2020.
- [24] P. Lu, "Entry guidance: A unified method," *Journal of Guidance, Control, and Dynamics*, vol. 37, no. 3, pp. 713–728, 2014.
- [25] H. K. Khalil, *Nonlinear Systems*, Third ed. Prentice Hall, 2002, chapter 3.
- [26] V. R. Makkapati, D. Maity, M. Dor, and P. Tsiotras, "C-DOC: Co-state desensitized optimal control," in *American Control Conference*, Denver, CO, July 2020, pp. 1761–1766.
- [27] Q. Wang and R. F. Stengel, "Robust nonlinear control of a hypersonic aircraft," *Journal of guidance, control, and dynamics*, vol. 23, no. 4, pp. 577–585, 2000.
- [28] O. U. Rehman, B. Fidan, and I. R. Petersen, "Robust minimax optimal control of nonlinear uncertain

- systems using feedback linearization with application to hypersonic flight vehicles," in *IEEE Conference on Decision and Control held jointly with Chinese Control Conference*, Shanghai, China, 2009, pp. 720–726.
- [29] X. Liu, Z. Shen, and P. Lu, "Entry trajectory optimization by second-order cone programming," *Journal of Guidance, Control, and Dynamics*, vol. 39, no. 2, pp. 227–241, 2016.
- [30] K. J. Murphy, R. J. Nowak, R. A. Thompson, B. R. Hollis, and R. Prabhu, "X-33 hypersonic aerodynamic characteristics," *Journal of Spacecraft and Rockets*, vol. 38, no. 5, pp. 670–683, 2001.
- [31] M. A. Patterson and A. V. Rao, "GPOPS-II: A MAT-LAB software for solving multiple-phase optimal control problems using hp-adaptive Gaussian quadrature collocation methods and sparse nonlinear programming," *ACM Trans. Mathematical Software*, vol. 41, no. 1, pp. 1:1–1:37, Oct. 2014.
- [32] T. E. Moore, "Space shuttle entry terminal area energy management," National Aeronautics and Space Administration, Tech. Rep. NASA-TM-104744, 1991.

#### **BIOGRAPHY**



Venkata Ramana Makkapati is a doctoral candidate in the School of Aerospace Engineering at the Georgia Institute of Technology. He applies techniques from optimal control, reinforcement learning, and differential games to address problems pertaining to autonomous vehicles, emphasizing safe path planning and airspace security. He received the B.Tech. from IIT Madras,

India in 2014, and the M.Tech. from IIT Kanpur, India in 2016, both in Aerospace Engineering.



Jack Ridderhof is a PhD student in aerospace engineering at the Georgia Institute of Technology. He received MS degrees in mathematics and aerospace engineering both from the Georgia Institute of Technology in 2019. His research focuses on stochastic control for spacecraft guidance. Jack is a NASA Space Technology Fellow.



Panagiotis Tsiotras is the David and Andrew Lewis Chair Professor in the D. Guggenheim School of Aerospace Engineering at the Georgia Institute of Technology (Georgia Tech), and the Director of the Dynamics and Controls Systems Laboratory (DCSL) in the same school, as well as Associate Director of the Institute for Robotics and Intelligent Machines at Georgia Tech. His research

interests include optimal control of nonlinear systems and ground, aerial and space vehicle autonomy. He is the recipient of the NSF CAREER award, the Outstanding Aerospace Engineer award from Purdue, and the Technical Excellence Award in Aerospace Control from IEEE. He is a Fellow of AIAA, IEEE, and AAS.



Joseph Hart is a senior member of the technical staff at Sandia National Laboratories. He received a PhD in Applied Mathematics from North Carolina State University in 2018. His research focuses on developing and applying optimization and uncertainty quantification algorithms for large-scale scientific and engineering applications.



Bart van Bloemen Waanders is a distinguished member of technical staff at Sandia National Laboratories. His research interests include large scale optimization, uncertainty quantification, sensitivity analysis, and engineering applications with a focus on impacting complex systems including additive manufacturing, geoscience, electromagnetics, and hypersonics.